

Ultra-Efficient Resistance Switching between Charge Ordered Phases in 1T-TaS₂ with a Single Picosecond Electrical Pulse

Rok Venturini^{1,2}, Anže Mraz^{1,3}, Igor Vaskivskiy¹, Yevhenii Vaskivskiy^{1,2}, Damjan Svetin^{1,4}, Tomaž Mertelj¹, Leon Pavlovič⁵, Jing Cheng⁶, Genyu Chen⁶, Priyanthi Amarasinghe⁷, Syed B. Qadri⁸, Sudhir B. Trivedi⁷, Roman Sobolewski^{6,9}, and Dragan Mihailovic^{1,4}

Affiliations

¹*Jožef Stefan Institute, Jamova 39, Ljubljana, SI-1000, Slovenia,*

²*Department of Physics, Faculty of Mathematics and Physics, University of Ljubljana, Jadranska 19, Ljubljana, SI-1000, Slovenia*

³*Faculty for Electrical Engineering, University of Ljubljana, Tržaška 25, SI-1000 Ljubljana, Slovenia*

⁴*CENN Nanocenter, Jamova 39, SI-1000 Ljubljana, SI-1000, Slovenia*

⁵*ELEP Electronics, Ljubljana, SI-1000, Slovenia*

⁶*Materials Science Program and Laboratory for Laser Energetics, University of Rochester, New York 14627, USA*

⁷*Brimrose Technology Corporation, Sparks, MD 21152, USA*

⁸*U.S. Naval Research Laboratory, Washington D.C., USA*

⁹*Department of Electrical and Computer Engineering and Department of Physics and Astronomy, University of Rochester, New York 14627, USA*

Keywords: resistance switching, 1T-TaS₂, picosecond electrical pulse, electro-optic sampling

Abstract text

Progress in high-performance computing demands significant advances in memory technology. Among novel memory technologies that promise efficient device operation on a sub-ns timescale, resistance switching between charge ordered phases of the 1T-TaS₂ has shown to be potentially useful for the development of high-speed, energy efficient non-volatile memory device. While ultrafast switching was previously reported with optical pulses, determination of the intrinsic speed limits of actual devices that are triggered by electrical pulses is technically challenging and hitherto still largely unexplored. A new optoelectronic “laboratory-on-a-chip”, designed for measurements of ultrafast memory switching, enables an accurate measurement

of the *electrical* switching parameters with 100 fs temporal resolution. A photoconductive response is used for ultrashort electrical pulse generation, while its propagation along a coplanar transmission line is detected using electro-optical sampling using a purpose-grown highly-resistive electro-optic (Cd,Mn)Te crystal substrate. By combining the transmission line and the 1T-TaS₂ device in a single optoelectronic circuit a *non-volatile* resistance switching with a single 1.9 ps electrical pulse is demonstrated, with an extremely small switching energy density per unit area $E_A = 9.4 \text{ fJ}/\mu\text{m}^2$. The experiments demonstrate ultrafast, energy-efficient circuits utilizing switching between non-volatile charge-ordered states offers a new technological platform for cryogenic memory devices.

Introduction

Memory speed and energy efficiency have become one of the major bottlenecks limiting advanced computer development¹. As a result, there has been significant interest in recent years to address this issue by exploring novel memory concepts, such as memristors², phase-change³, ferroelectric⁴ and magnetic memory⁵ devices. One of the emerging new platforms for non-volatile storage of information is switching between distinct charge configurations or charge density wave (CDW) phases of a material. Such phases, where the electronic density is spatially modulated in the crystal, are common in low-dimensional materials and have attracted a lot of interest from the point of view of fundamental physics as their formation is still poorly understood^{6,7}. When CDW order in a material is disrupted, for example by hydrostatic pressure⁸⁻¹⁰ or chemical doping¹¹⁻¹³, novel material functionality can emerge, such as a large change of electrical resistance or an appearance of a superconducting state. Optical, THz, or electrical pulsed excitations can also be used to drive the material towards a novel charge order¹⁴⁻¹⁷. However, the usefulness of such switching has long been limited, as excited CDW states are typically not stable, and cannot be used for non-volatile devices¹⁸⁻²⁰.

The material used in this study is 1T-TaS₂, a layered transitional metal dichalcogenide with a rich phase diagram exhibiting several distinct CDW phases. At room temperature the material is in a metallic nearly commensurate (NC) CDW phase state, from which an insulating commensurate (C) CDW state forms below around 180 K⁷. Either a laser or an electrical pulse excitation can drive the crystal from the C state, to a so-called hidden (H) state with a complex network of domains separated by domain walls that is distinct from the NC state^{14,15,21-23}. The H state is metastable and is not observed in the equilibrium phase diagram of the material. Owing to topological protection, the new state is remarkably stable at low temperatures²³.

Relaxation back to the C state is temperature dependent, but the state is stable on laboratory timescales at temperatures lower than 20 K^{24–26}. Robust memory device operation by switching between the two phases with electrical pulses of various lengths has already been presented^{15,21,25}. Optical experiments show that once the transition between the charge ordered phases is triggered, it can stabilize into new order within 400 fs²⁶. If picosecond *electrical* pulses could trigger a resistance-switching charge reconfiguration, it may be possible to write to such memory devices at THz frequencies. Due to limitations of electrical generators and dispersion of cryostat cables, demonstration of electronic device operation on a such short timescale is currently still challenging. For example, electrical switching with 16 ps electrical pulses applied to the cryostat cable was recently demonstrated²⁵, however due to above-mentioned constraints, electrical pulse length and shape at the sample position are not known.

A way to overcome these issues is by *in-situ* generation and detection of ultrashort electrical pulses on-a-chip by a femtosecond laser pulse and then propagating electrical pulses along a coplanar transmission line (TL) to the device. While this technology is well known^{27–30} and has been used to perform switching of superconducting Josephson junctions³¹ and circuits^{32,33}, interest in this topic has recently re-emerged with ultrafast electronic studies of topological states of matter^{34,35} and magnetization reversal^{36,37}. In our case, we embedded a 1T-TaS₂ device in the TL on a substrate that is both photoconductive and exhibits an electro-optic (EO) effect, so in addition to resistance measurement, ultrashort electrical pulses can be generated and sampled anywhere along the TL. The EO detection can easily be calibrated to a known voltage, so a reading of the picosecond pulse voltage can be used to accurately calculate the pulse energy. This offers a significant advantage over the experiments that use either a photoconductive gap or an antenna for detection, where calibration would be more difficult and the energy for switching can only be given as a high upper limit estimate^{36,37}.

Ultrafast experiment-on-a-chip

Figure 1 shows the operating principles of the lab-on-a-chip TL circuit used in our experiment. The TL itself, fabricated on a Cd_{0.55}Mn_{0.45}Te (CMT) substrate, is shown in Figure 1b. The three electrodes are marked A, B and C, where A is grounded, B is used to source DC voltage, and C is used to measure the resistance of the exfoliated 32 nm thick flake of 1T-TaS₂. A crucial part of the circuit is the 22 μm wide gap between the TL electrodes B and C that acts as a capacitor which prevents DC current flow through the 1T-TaS₂ flake when a high DC bias voltage is applied between leads A and B, while allowing short photogenerated electrical pulses

to be transmitted with low attenuation. The entire TL is relatively long (4 mm, not shown) in order to reduce the effect of pulse reflections from ends of the electrodes.

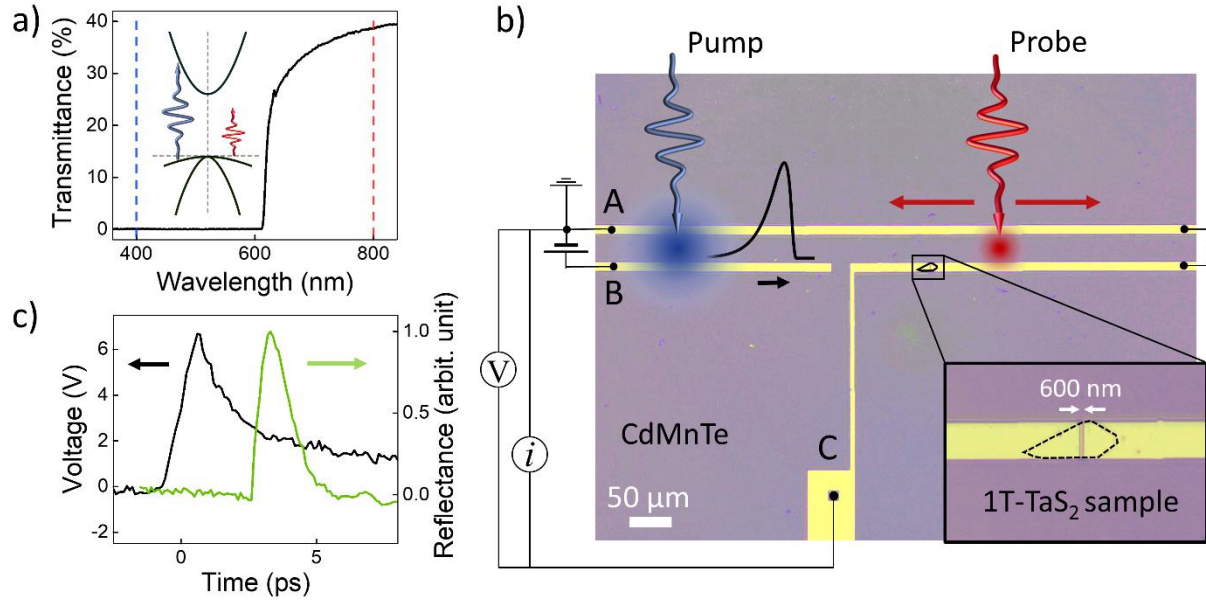


Figure 1. a) The absorption spectrum of the CMT in relation to the pump beam (blue) and the probe beam (red). An inset shows a schematic of the CMT band structure around $k=0$ point with a direct bandgap of 2.0 eV³⁸ b) A microscope image of the fabricated TL circuit over the exfoliated 1T-TaS₂ crystal with the pump beam (blue) and the span of the probe beam (red) positions. Voltmeter and current source connect the electrodes A and C for measurement of the 1T-TaS₂ crystal resistance, while voltage source is connected between the electrodes A and B to create a high DC bias voltage. c) A pump-probe reflectance measurement of the CMT crystal by spatially overlapping both beams away from the TL circuit (green). The picosecond electrical pulse with the FWHM of 1.9 ps detected by positioning probe beam 40 μm in front of the 1T-TaS₂ and pump beam 120 μm above the gap between B and C electrodes (black).

To facilitate both electrical pulse generation and their electro-optical detection on the same substrate chip, we use a vanadium-doped $\text{Cd}_{0.55}\text{Mn}_{0.45}\text{Te}$ (CMT) single crystal substrate grown by the vertical Bridgman method³⁹. This diluted magnetic semiconductor has a chemically tunable direct band gap, controlled by Mn content³⁸. Its band gap, $E_g = 2.02$ eV, allows optical absorption and photocarrier generation using optical photons with $\lambda < 600$ nm, while passing red light ($\lambda \geq 700$ nm) without absorption. E_g of our substrate was determined by optical transmittance measurement (Figure 1a) and is in agreement with theoretical expectations³⁸.

Vanadium doping results in highly resistive crystals with a carrier lifetime below 2 ps measured using two-color (400 nm/800 nm) femtosecond pump-probe measurements (Figure 1c).

By applying a DC voltage between electrodes A and B (without laser illumination) we observe ohmic behavior of the dark current with a resistance greater than 10^9 ohm. In addition, the CMT substrate has its EO tensor component along the [001] direction so photogenerated electric-field transient propagating in the TL fabricated on the (110) plane can be measured via the Pockels effect³⁰. We can thus sample the propagating electric fields by an 800 nm, intra-gap (1.55 eV), laser beam focused between the TL coplanar lines in the transmission mode as shown in Figure 1a. Both the excitation of the electrical pulses with 400-nm (3.1 eV) pump optical pulses and the EO sampling by 800-nm probe pulses is done with 100 fs laser pulses at a 250 kHz repetition rate. An acousto-optic modulator positioned in the laser beam allows for single pulse picking, when necessary. The temporal evolution of an electrical pulse is measured by adjusting a time delay between the pump and probe pulses, which also allows us to measure the speed of propagation c along the TL.

Experimental results

We first present characterization of the ultrashort electrical pulses generated on the TL circuit. A slightly defocused *pump* laser beam is used to illuminate the CMT substrate between electrodes A and B. By using a low laser pump power of 1 mW (a fluence of 0.3 mJ/cm^2), and moderate DC voltage of 76 V between electrodes A and B, sufficiently low amplitude electrical pulses are created that avoid damage or switching of CDW state in the 1T-TaS₂ crystal. To minimize dispersion effects that broaden the electrical pulses, we focus the *probe* beam relatively close (40 μm) to the 1T-TaS₂ crystal (Figure 1 b) in order to give an accurate measurement of the electrical pulse shape close to the device. In this configuration, we measure the full width at half maximum (FWHM) of the electrical pulse of 1.9 ps (Figure 1c). Repeating the experiment with the probe beam 100 μm *after* the 1T-TaS₂ crystal we observe an electrical pulse of the same shape (Figure 3a). This demonstrates that the electrical pulse shape is not significantly changed by the sample, but the amplitude is lowered slightly due to high-frequency losses³⁰. We also observe reflections from the end of the TL 25 ps after the initial pulse, but their amplitude is 3-times lower, due to high-frequency losses during 3 mm of travel to the end of the TL and back³⁰. Therefore, we can conclude that the reflections have no significant role in the switching experiment.

For ultrafast resistance switching of the 1T-TaS₂ device, the chip is cooled from room temperature to 16 K while the DC resistance of the device is continuously measured (Figure 2). At 16 K, as before, we position the pump beam between the TL electrodes A and B, and the probe after the 1T-TaS₂ crystal, and measure the propagating electrical pulse shape with low DC voltage to verify that the pulse shape is unchanged. Without the pump illumination of the substrate, we increase the DC voltage to 220 V and the pump power to 17.1 mW (5.5 mJ/cm²). After verifying that the crystal resistance hasn't changed, we use an acousto-optic modulator to pick a single optical pump pulse that excites a single picosecond electrical pulse. After a *single pulse* exposure, we observe a large drop in the resistance as shown on Figure 2. The drop in the electrical resistance is consistent with a charge reconfiguration from the C to the H state which was previously observed with longer electrical pulses^{15,40}. During heating of the crystal back to room temperature, we observe an increase in the sample resistance between 50 K and 100 K which is associated with relaxation of the metastable H state back to the C state^{14,24}. The cycle of cooling the crystal, switching by a single pulse and then erasing the H state by heating was sequentially repeated many times, demonstrating consistency of single-shot ultrafast resistance switching.

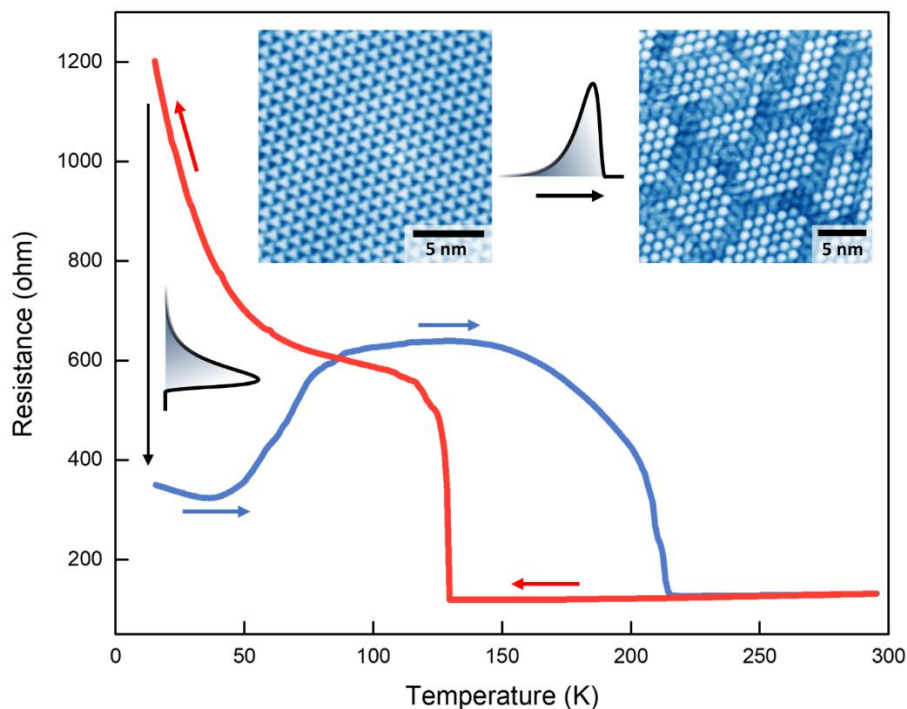


Figure 2. Resistance of the 1T-TaS₂ upon cooling (red). Resistance switching of the crystal by a single 1.9 ps electrical pulse at 16 K (black arrow). Heating of the crystal back to room temperature (blue). Inset figures are scanning tunnelling microscope images of the C state (left) and the H state (right) from ref. ⁴¹.

In all further switching experiments the temperature is kept below 20 K with the 1T-TaS₂ device operation in non-volatile mode. Figure 3b presents how the 1T-TaS₂ crystal resistance changes in response to repeated single pulse excitation. After each single pulse we measure the resistance, and wait 1 min before applying the next pulse. The largest resistance change is caused by the initial pulse, with the next few pulses gradually lowering the resistance towards saturation. If the amplitude of the pulses is below the threshold, we do not observe any change in the crystal resistance. Even after applying 10⁸ pulses at a 250 kHz repetition rate at 60 V DC bias, there was no detectable resistance change of the 1T-TaS₂ device. This demonstrates that the threshold for switching is very sharp and the device behavior is robust even for such short pulses.

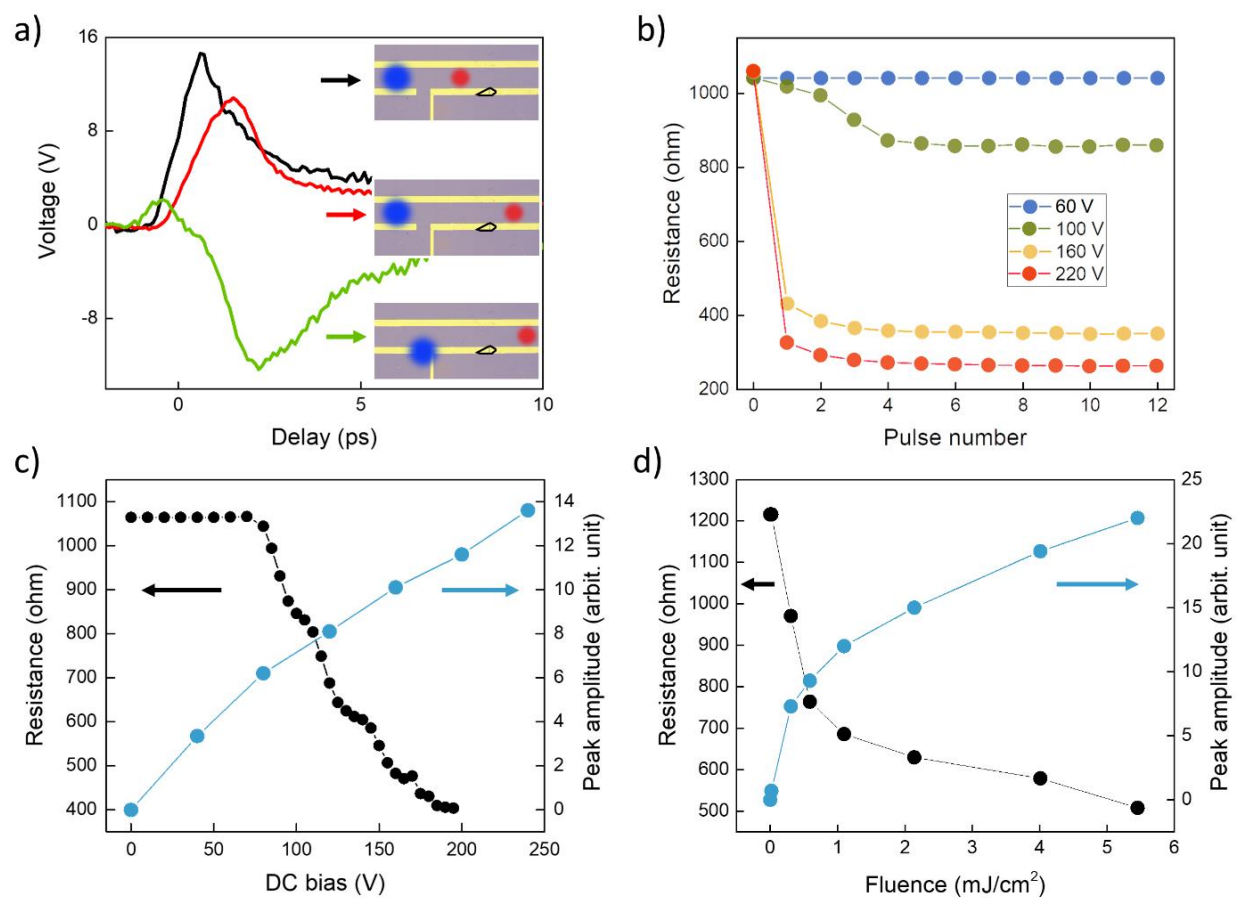


Figure 3. a) Shape of the picosecond electrical pulse sampled by the probe beam 40 μm before (black) and 100 μm after the sample (red). Additionally, it is possible to position pump beam on a gap to create an electrical pulse with a reversed polarity (green). Inset figures show the optical microscope image of the TL with the schematic of the pump (blue) and probe (red) beam positions. b) Build-up effect on the 1T-TaS₂ resistance by applying multiple electrical pulses one by one for different DC bias voltages. c) Decreasing electrical resistance of the 1T-TaS₂ crystal after applying picosecond pulses with increasing the DC bias (black) at fixed pump fluence of 5.5 mJ/cm^2 . Picosecond electrical

pulse amplitude scaling with the DC bias (blue). d) Decreasing electrical resistance of the 1T-TaS₂ crystal after applying picosecond pulses with an increasing pump fluence at the DC bias voltage of 150 V (black). Electrical pulse amplitude scaling with the pump fluence (blue).

Next, we show how the picosecond electrical pulse amplitude is affected by changing the DC bias voltage and the pump fluence. As expected, the pulse amplitude (measured at fixed pump fluence of 0.4 mJ/cm²) increases almost linearly with increasing the DC voltage (Figure 3c). Then, we measure electrical resistance of the 1T-TaS₂ after applying picosecond pulses with increasing the DC bias at fixed pump fluence of 5.5 mJ/cm². The resistance is unchanged for picosecond pulse amplitude below a certain threshold and then it starts to continuously decrease with increasing pulse amplitude. We then perform an experiment where we fix the DC bias voltage at 60 V and increase pump fluence (Figure 3d). We observe a saturation of the pulse amplitude with increasing pump fluence, consistent with previous results for the CMT substrate³⁰. Furthermore, no change of the picosecond pulse shape is observed by changing the DC bias and/or the pump fluence within the explored intervals of 0-250 V and 0-5.5 mJ/cm², respectively.

Finally, we perform a slightly modified electrical switching experiment where instead of pump beam being between electrodes A and B we focus the pump beam on the gap between electrodes B and C (Figure 3a). We observe a similar pulse, however, the polarity of the electrical pulse is now reversed. We repeat the switching experiment presented in Figure 3c with the electrical pulses of reversed polarity and obtain very similar switching results.

Discussion

The present experiments suggest that resistance switching occurs only if the amplitude of the picosecond electrical pulse exceeds a certain threshold, in agreement with previous experiments with longer electrical pulses^{15,25}. We see very similar switching behavior for electrical pulses of both positive and negative polarity. This is not surprising as the resistance switching in the 1T-TaS₂ is based on electrical current induced charge reordering^{15,25,40}, and is not dependent on the pulse polarity or the direction of the current flow through the crystal.

From the Figure 3a it is clear that only a small fraction of the picosecond pulse energy is absorbed in the 1T-TaS₂ crystal while the majority of the pulse propagates along the TL past the crystal. Because the absorbed fraction is small, spot-to-spot variation in EO signal (~30%)

prevent us from accurately measuring the dissipated energy of the pulse in the 1T-TaS₂ crystal by directly comparing the measured EO signals before and after the crystal.

Instead, to estimate the energy of switching, we employ 3D electromagnetic simulation software (Ansys HFSS). First, we simulate a straight coplanar TL without any gaps (or sample). For the CMT substrate we use the dielectric constant obtained from the parent compound⁴². From the simulation we obtain the TL impedance of 125 ohms and a speed of pulse propagation of $c = 1.25 \times 10^8$ m/s. The calculated speed of electrical pulse propagation is checked by measuring the time of flight of the pulse. This is done by changing the separation between pump and EO probe beams. The measured speed of propagation is 1.2×10^8 m/s, which closely matches the value obtained from the simulation. Using the calculated impedance value and experimentally measured voltage between the electrodes, we calculate the energy of the propagating picosecond electrical pulse at the threshold for switching $E_T = \int \frac{U_{TL}^2(t)}{Z} dt = 0.59$ pJ, where U_{TL} is voltage of the electrical pulse between the TL electrodes and Z is impedance of the TL. The integral is extended to 7 ps to include also the pulse tail.

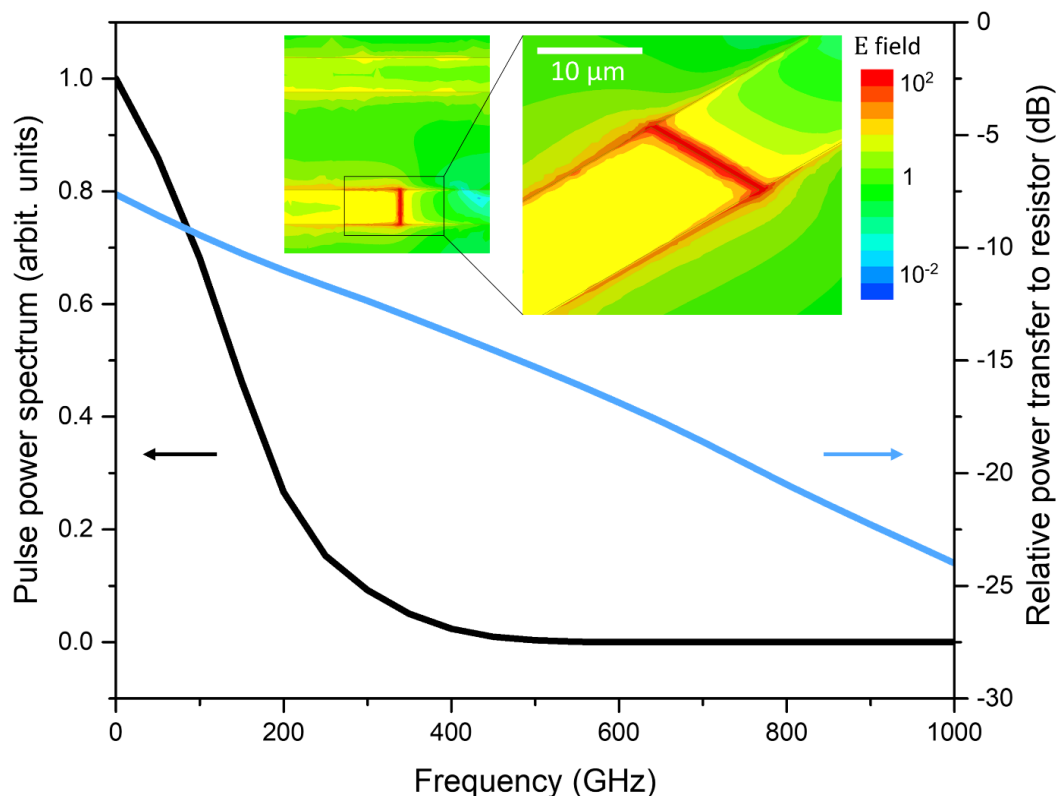


Figure 4. Power spectrum of the picosecond electrical pulse (black line) and relative power transfer of the propagating pulse to the 1T-TaS₂ crystal obtained from the simulation (blue line). The insets show the calculated electric field relative to the field between TL electrodes simulated at the 100 GHz frequency.

Next, to estimate the actual switching energy, we modify the TL in the simulation by inserting a 600 nm gap with a 1100 ohm 2D resistor to represent a 1T-TaS₂ crystal in the high resistance state (inset to Figure 4). Based on the microwave simulation of the relative power transfer to the resistor inside the gap, we observe only a weak coupling of the propagating pulse to the resistor (sample) that is also frequency dependent (Figure 4). The dissipated energy is calculated by multiplying the power spectrum of the picosecond electrical pulse (Figure 4) with the power spectrum of the losses inside the resistor, and then integrating over frequency. We find that 11.5 % of electrical pulse energy is dissipated inside the 1T-TaS₂ crystal. For the electrical pulse at the switching threshold this corresponds to a switching energy of 68 fJ. Note that this is still an upper bound, since it assumes that all the energy is dissipated in the switching process over the entire frequency range, which is not necessarily the case. Optical experiments indicate that the transition to a low resistance state is triggered already within 400 fs after the optical pulse arrival, which means that only the first part of the electrical pulse might be responsible for switching and the energy from the tail of the electrical pulse only contributes to heating of already switched crystal.

By using measured dimensions of the 1T-TaS₂ crystal between the electrodes, the estimated switching energy of 68 fJ corresponds to an energy density per unit volume $E_V = 0.3 \text{ pJ}/\mu\text{m}^3$, or an energy per unit area $E_A = 9.4 \text{ fJ}/\mu\text{m}^2$. Thus, as far as we are aware, 1T-TaS₂ devices exhibit the lowest switching energy per unit area and fastest switching time for any fast memory device reported until now²⁵. Previous electrical switching experiments in 1T-TaS₂ have shown that both switching voltage and energy scale linearly with device size²⁵. Considering the large volume of the device used in the present experiments, the energy for resistance switching could potentially be reduced by more than an order of magnitude by fabricating smaller devices.

Conclusion

The lab-on-a-chip experiments demonstrate that non-volatile switching with large resistance contrast is possible in 1T-TaS₂ devices approaching terahertz frequencies, limited presently by the carrier recombination lifetime of the photoconductive switch. Direct measurement of the voltage propagation on the transmission line circuit with high temporal resolution is the key to demonstrating ultrafast and energy efficient switching, even in relatively large devices, approaching the optical 400 fs switching limit²⁶. Considering that the devices operate well at low temperatures, charge configuration memory elements based on the resistance switching of 1T-TaS₂ could fit well with the emerging technologies that operate at cryogenic temperatures,

such as superconducting⁴³ circuits. With the ability to grow few layer crystals by epitaxial growth^{44,45}, devices based on charge configuration switching could provide a much-needed ultrafast energy efficient solution for classical information storage in both classical and quantum computing environments.

Methods

CMT crystal preparation. Vanadium-doped $\text{Cd}_{0.55}\text{Mn}_{0.45}\text{Te}$ (CMT) single crystal were grown by a vertical Bridgman technique³⁹. CMT single crystals were synthesized using high purity Cd and Te (99.9999% pure) and 99.99% pure Mn, and V, all procured from Alfa Aesar. The pre-synthesized material was loaded into a pre-cleaned, baked, and graphitized fused silica ampoule, and vacuum sealed (10^{-6} torr). After the crystal growth, the ingot was carefully removed from the ampoule and cleaved in (011) direction. The X-ray diffraction analysis was performed to identify all three crystallographic directions, lattice parameter a and the composition of the grown crystals. For the analysis, a Rigaku four-circle diffractometer with an 18-kW rotating-anode Cu source was used. After all three directions were determined, rectangular substrates were prepared. The large (011) surfaces of the samples were polished mechanically to optical finish.

Transmission line and electrical measurements. First, the 32 nm thick flake exfoliated from bulk 1T-TaS₂ crystal was deposited on the CMT substrate and its thickness was determined by the AFM. Next, the TL circuit was fabricated with e-beam lithography using an e-beam evaporator with the deposition of 3 nm of Cr followed by 160 nm of Au. TL electrodes A and B are 12 μm wide and 34 μm apart, while the width of electrode C is 6 μm . The crystal of 1T-TaS₂ is positioned 100 μm from the C electrode, with the TL gap of 0.6 μm above the crystal. The resistance of the 1T-TaS₂ crystal was measured by sourcing 100 nA of current between electrodes A and C and measuring the voltage drop across the crystal. Measurement was performed with a Keithley 6221 current source and 2182A voltmeter in the delta mode. The capacitance C of the 1T-TaS₂ device gap is a combination of the dielectric constant of the substrate and the sample. Using a conservative estimate of the effective dielectric constant $\epsilon = 10$, we estimate $C \approx 3 \times 10^{-16}$ F. The effective RC constant does not limit the observed time-response in the experiment.

Optical setup details. Excitation and sampling of the ultrashort electrical pulses is done by means of ~ 100 fs laser pulses at a 250 kHz repetition rate. An acousto-optic modulator positioned in the laser beam allows for single pulse picking, when necessary. The laser beam

is split by the 90/10 beam splitter into two branches. The 800 nm probe beam is used to detect the EO signal in transmission by measuring the change in beam polarization with a Wollaston prism and a pair of photodiodes. The polarization of the probe beam is adjusted to be at an angle of 45 degrees with respect to the TL electrodes on the CMT to observe a maximum EO signal. We calibrate the EO response to a voltage between the TL electrodes with a 0.5 V sine wave voltage applied between contacts A and B. To avoid error due to spot-to-spot EO signal variation, we use the same spot for both measuring the picosecond electrical pulse and the 0.5 V sine wave used for calibration. This calibration was done on a separate CMT crystal, so there might be some systematic error in the reported voltages due to crystal variation. To obtain the 400 nm pump, we frequency double the 800 nm laser beam in a BBO crystal. The pump beam is modulated by a mechanical chopper at a frequency of 2865 Hz, which is used as a reference for a lock-in detection of the probe beam signal.

Conflict of interest: The authors declare no competing interests.

Acknowledgment

The authors would like to thank Jan Ravnik for help with building an optical setup. The work at the Jožef Stefan Institute was supported by the Slovenian Research Agency (No. P1-0040, No. N1-0092, No. J1-2455, R.V. to No. PR-10496, A.M. to No. PR-08972, D.S. to No. I0-0005), Slovene Ministry of Science (No. Raziskovalci-2.1-IJS-952005), and ERC PoC (No.GA767176). The work in Rochester and Brimrose was supported by the DOE STTR 2021 Phase 1 grant # DE-SC0021468. We thank the CENN Nanocenter for the use of the AFM and the FIB.

References

1. Zidan MA, Strachan JP, Lu WD. The future of electronics based on memristive systems. *Nat Electron*. 2018;1(1):22-29. doi:10.1038/s41928-017-0006-8
2. Pi S, Li C, Jiang H, et al. Memristor crossbar arrays with 6-nm half-pitch and 2-nm critical dimension. *Nat Nanotechnol*. 2019;14(1):35-39. doi:10.1038/s41565-018-0302-0
3. Loke D, Lee TH, Wang WJ, et al. Breaking the Speed Limits of Phase-Change Memory. *Science*. 2012;336(6088):1566-1569. doi:10.1126/science.1221561
4. Chanthbouala A, Crassous A, Garcia V, et al. Solid-state memories based on ferroelectric tunnel junctions. *Nat Nanotech*. 2012;7(2):101-104. doi:10.1038/nnano.2011.213
5. Vedmedenko EY, Kawakami RK, Sheka DD, et al. The 2020 magnetism roadmap. *J Phys D: Appl Phys*. 2020;53(45):453001. doi:10.1088/1361-6463/ab9d98
6. Gruner G. The dynamics of charge-density waves. *Rev Mod Phys*. 1988;60(4):53.

7. Rossnagel K. On the origin of charge-density waves in select layered transition-metal dichalcogenides. *J Phys Condens Matter*. 2011;23(21):213001. doi:10.1088/0953-8984/23/21/213001
8. Sipos B, Kusmartseva AF, Akrap A, Berger H, Forró L, Tutiš E. From Mott state to superconductivity in 1T-TaS₂. *Nat Mater*. 2008;7(12):960-965. doi:10.1038/nmat2318
9. Kusmartseva AF, Sipos B, Berger H, Forró L, Tutiš E. Pressure Induced Superconductivity in Pristine 1T-TiSe₂. *Phys Rev Lett*. 2009;103(23):236401. doi:10.1103/PhysRevLett.103.236401
10. Berthier C, Molinié P, Jérôme D. Evidence for a connection between charge density waves and the pressure enhancement of superconductivity in 2H-NbSe₂. *Solid State Commun*. 1976;18(9-10):1393-1395. doi:10.1016/0038-1098(76)90986-8
11. Morosan E, Zandbergen HW, Dennis BS, et al. Superconductivity in Cu_xTiSe₂. *Nat Phys*. 2006;2(8):544-550. doi:10.1038/nphys360
12. Li LJ, Lu WJ, Zhu XD, Ling LS, Qu Z, Sun YP. Fe-doping-induced superconductivity in the charge-density-wave system 1T-TaS₂. *EPL*. 2012;97(6):67005. doi:10.1209/0295-5075/97/67005
13. Liu Y, Ang R, Lu WJ, Song WH, Li LJ, Sun YP. Superconductivity induced by Se-doping in layered charge-density-wave system 1T-TaS_{2-x}Se_x. *Appl Phys Lett*. 2013;102(19):192602. doi:10.1063/1.4805003
14. Stojchevska L, Vaskivskiy I, Mertelj T, et al. Ultrafast Switching to a Stable Hidden Quantum State in an Electronic Crystal. *Science*. 2014;344(6180):177-180. doi:10.1126/science.1241591
15. Vaskivskiy I, Mihailovic IA, Brazovskii S, et al. Fast electronic resistance switching involving hidden charge density wave states. *Nat Commun*. 2016;7:11442. doi:10.1038/ncomms11442
16. Kogar A, Zong A, Dolgirev PE, et al. Light-induced charge density wave in LaTe₃. *Nat Commun*. 2020;16(2):159-163. doi:10.1038/s41567-019-0705-3
17. Yoshikawa N, Suganuma H, Matsuoka H, et al. Ultrafast switching to an insulating-like metastable state by amplitudon excitation of a charge density wave. *Nat Phys*. 2021;17(8):909-914. doi:10.1038/s41567-021-01267-3
18. Mohammadzadeh A, Baraghani S, Yin S, Kargar F, Bird JP, Balandin AA. Evidence for a thermally driven charge-density-wave transition in 1T-TaS₂ thin-film devices: Prospects for GHz switching speed. *Appl Phys Lett*. 2021;118(9):093102. doi:10.1063/5.0044459
19. Wang X, Song Z, Wen W, et al. Potential 2D Materials with Phase Transitions: Structure, Synthesis, and Device Applications. *Adv Mater*. 2019;31(45):1804682. doi:10.1002/adma.201804682
20. Liu G, Debnath B, Pope TR, Salguero TT, Lake RK, Balandin AA. A charge-density-wave oscillator based on an integrated tantalum disulfide–boron nitride–graphene device operating at room temperature. *Nature Nanotech*. 2016;11(10):845-850. doi:10.1038/nnano.2016.108
21. Yoshida M, Suzuki R, Zhang Y, Nakano M, Iwasa Y. Memristive phase switching in two-dimensional 1T-TaS₂ crystals. *Sci Adv*. 2015;1(9):e1500606. doi:10.1126/sciadv.1500606
22. Ma L, Ye C, Yu Y, et al. A metallic mosaic phase and the origin of Mott-insulating state in 1T-TaS₂. *Nat Commun*. 2016;7:10956. doi:10.1038/ncomms10956

23. Gerasimenko YA, Karpov P, Vaskivskiy I, Brazovskii S, Mihailovic D. Intertwined chiral charge orders and topological stabilization of the light-induced state of a prototypical transition metal dichalcogenide. *npj Quantum Mater.* 2019;4(1):1-9. doi:10.1038/s41535-019-0172-1
24. Vaskivskiy I, Gospodaric J, Brazovskii S, et al. Controlling the metal-to-insulator relaxation of the metastable hidden quantum state in 1T-TaS₂. *Sci Adv.* 2015;1(6):e1500168-e1500168. doi:10.1126/sciadv.1500168
25. Mraz A, Venturini R, Diego M, et al. Energy efficient manipulation of topologically protected states in non-volatile ultrafast charge configuration memory devices. *arXiv:210304622*. Published online March 8, 2021. Accessed July 26, 2021. <http://arxiv.org/abs/2103.04622>
26. Ravnik J, Vaskivskiy I, Mertelj T, Mihailovic D. Real-time observation of the coherent transition to a metastable emergent state in 1T-TaS₂. *Phys Rev B.* 2018;97(7):075304. doi:10.1103/PhysRevB.97.075304
27. Auston DH. Picosecond optoelectronic switching and gating in silicon. *Appl Phys Lett.* 1975;26(3):101-103. doi:10.1063/1.88079
28. Ketchen MB, Grischkowsky D, Chen TC, et al. Generation of subpicosecond electrical pulses on coplanar transmission lines. *Appl Phys Lett.* 1986;48(12):751-753. doi:10.1063/1.96709
29. Mourou GA, Meyer KE. Subpicosecond electro-optic sampling using coplanar strip transmission lines. *Appl Phys Lett.* 1984;45(5):492-494. doi:10.1063/1.95312
30. Serafini J, Hossain A, James RB, et al. Photoconductive and electro-optic effects in (Cd,Mg)Te single crystals measured in an experiment-on-chip configuration. *Appl Phys Lett.* 2017;111(1):011108. doi:10.1063/1.4993155
31. Dykaar DR, Sobolewski R, Hsiang TY. Picosecond switching dynamics of a Josephson tunnel junction. *IEEE Trans Magn.* 1989;25(2):1392-1395. doi:10.1109/20.92555
32. Hegmann FA, Jacobs-Perkins D, Wang C -C., et al. Electro-optic sampling of 1.5-ps photoresponse signal from YBa₂Cu₃O_{7-δ} thin films. *Appl Phys Lett.* 1995;67(2):285-287. doi:10.1063/1.114784
33. Adam R, Currie M, Williams C, Sobolewski R, Harnack O, Darula M. Direct observation of subpicosecond single-flux-quantum generation in pulse-driven Y-Ba-Cu-O Josephson junctions. *Appl Phys Lett.* 2000;76(4):469-471. doi:10.1063/1.125790
34. Kastl C, Karnetzky C, Karl H, Holleitner AW. Ultrafast helicity control of surface currents in topological insulators with near-unity fidelity. *Nat Commun.* 2015;6(1):6617. doi:10.1038/ncomms7617
35. McIver JW, Schulte B, Stein FU, et al. Light-induced anomalous Hall effect in graphene. *Nat Phys.* 2020;16(1):38-41. doi:10.1038/s41567-019-0698-y
36. Yang Y, Wilson RB, Gorochon J, Lambert CH, Salahuddin S, Bokor J. Ultrafast magnetization reversal by picosecond electrical pulses. *Sci Adv.* 2017;3(11):e1603117. doi:10.1126/sciadv.1603117
37. Jhuria K, Hohlfeld J, Pattabi A, et al. Spin-orbit torque switching of a ferromagnet with picosecond electrical pulses. *Nat Electron.* 2020;3(11):680-686. doi:10.1038/s41928-020-00488-3

38. Furdyna JK. Diluted magnetic semiconductors. *J Appl Phys.* 1988;64(4):R29-R64. doi:10.1063/1.341700
39. Trivedi SB, Wang CC, Kutcher S, Hommerich U, Palosz W. Crystal growth technology of binary and ternary II–VI semiconductors for photonic applications. *J Cryst Growth.* 2008;310(6):1099-1106. doi:10.1016/j.jcrysgro.2007.12.032
40. Mihailovic D, Svetin D, Vaskivskiy I, Venturini R, Lipovšek B, Mraz A. Ultrafast non-thermal and thermal switching in charge configuration memory devices based on 1T-TaS₂. *Appl Phys Lett.* 2021;119(1):013106. doi:10.1063/5.0052311
41. Vodeb J, Kabanov VV, Gerasimenko YA, et al. Configurational electronic states in layered transition metal dichalcogenides. *New J Phys.* 2019;21(8):083001. doi:10.1088/1367-2630/ab3057
42. Perkowitz S, Thorland RH. Far-infrared study of free carriers and the plasmon-phonon interaction in CdTe. *Phys Rev B.* 1974;9(2):545-550. doi:10.1103/PhysRevB.9.545
43. Holmes DS, Ripple AL, Manheimer MA. Energy-Efficient Superconducting Computing—Power Budgets and Requirements. *IEEE Trans Appl Supercond.* 2013;23(3):1701610-1701610. doi:10.1109/TASC.2013.2244634
44. Chen Y, Ruan W, Wu M, et al. Strong correlations and orbital texture in single-layer 1T-TaSe₂. *Nat Phys.* 2020;16(2):218-224. doi:10.1038/s41567-019-0744-9
45. Wang X, Liu H, Wu J, et al. Chemical Growth of 1T-TaS₂ Monolayer and Thin Films: Robust Charge Density Wave Transitions and High Bolometric Responsivity. *Adv Mater.* 2018;30(38):1800074. doi:10.1002/adma.201800074